

# DELTA LAUNCH VEHICLE ISOGRID STRUCTURE NASTRAN ANALYSIS

By Daniel J. Knighton

NASA Goddard Space Flight Center

## SUMMARY

The purpose of this paper is to present the varied structural analysis applications of NASTRAN on the new isogrid<sup>1</sup> structure of the Delta launch vehicle. Isogrid is a method employed to stiffen the booster cylindrical shell surface by integrally machining ribs and skin from one piece of metal. The ribs are arranged in a repetitive equilateral triangular pattern; this results in a structural surface whose stiffness is orthogonally isotropic. For that structure both static and general instability buckling analysis will be described and the theoretical results will be compared to test data. One of the parameters that has been included in this analysis is the effect of pressure loadings on the buckling allowable load. In addition, a description of a supplementary GSFC-originated computer program, without which this analysis could not have been performed, will be presented.

## INTRODUCTION

A brief description of the Delta launch vehicle and its performance advancements will be given with specific attention focused on the IBM 360/95 computer analysis of the recently innovated Delta external isogrid shell structure. The NASA Structural Analysis (NASTRAN) program has been successfully employed to (1) verify the isotropic property of isogrid, (2) show the variation in deflections and detail stress levels depending on loading versus the orientation of isogrid, (3) perform as an engineering liaison tool, and (4) determine the general instability buckling allowables for isogrid tank structures.

---

<sup>1</sup>Isogrid structure concept was developed for Delta by McDonnell Douglas in 1970.

## SYMBOLS

$a'$	side of isogrid triangle, cm (in.)
A	area, $\text{cm}^2$ (in.)
a, b	locations of CBAR
CBAR	NASTRAN bar element
CTRIA2	NASTRAN triangular plate element
d	rib height, cm (in.)
D	diameter of cylinder, cm (in.)
E	Young's modulus of elasticity, $\text{kN/m}^2$ (psi)
$\bar{E}$	isogrid modulus, $\text{kN/m}^2$ (psi)
f	force, N (lb)
$f_{rc}$	rib-allowable compression stress, $\text{kN/m}^2$ (psi)
$f_{sb}$	skin-allowable compression stress, $\text{kN/m}^2$ (psi)
F	force, N (lb)
G	modulus of rigidity, $\text{kN/m}^2$ (psi)
h	height of isogrid triangle, cm (in.)
I	moment of inertia, $\text{cm}^4$ (in. <sup>4</sup> )
J	polar moment of inertia, $\text{cm}^4$ (in. <sup>4</sup> )
K	form factor of cross section
$[K_{aa}]$	elastic stiffness
$[K_{aa}^d]$	differential stiffness
l	length, cm (in.)
m	moment, N-m (in.-lb)
M	bending moment, N-m (in.-lb)
$N_{GI}$	isogrid general instability allowable load, $\text{kN/m}$ (lb/in.)

$N_{rc}$	rib-allowable compression or crippling load, kN/m (lb/in.)
$N_{sb}$	skin-allowable compression or buckling load, kN/m (lb/in.)
$N_x$	equivalent compression load, kN/m (lb/in.)
$p$	pressure, kN/m <sup>2</sup> (psi)
$P$	applied axial load, N (lb)
$R$	radius, cm (in.)
$\bar{t}$	equivalent skin thickness, cm (in.)
$t_r$	rib thickness, cm (in.)
$t_s$	skin thickness, cm (in.)
$t_{wt. eq.}$	weight equivalent thickness (accounting for weld land and/or edge panel design)
$T$	torque, N-m (in.-lb)
$u$	linear displacement of CBAR grid point
$\{u\}$	eigenvector
$V$	shear, N (lb)
$dV$	infinitesimal element volume
$\epsilon_{xx}, \epsilon_{yy}$	extensional strain, cm/cm (in./in.)
$\epsilon_{xy}$	shear strain, cm/cm (in./in.)
$\theta$	rotation of CBAR grid point
$\lambda$	eigenvalue
$\nu$	Poisson's ratio
$\sigma_x, \sigma_y$	axial stress of isogrid in x, y directions, kN/m <sup>2</sup> (psi)
$\tau_{xy}$	shear stress, kN/m <sup>2</sup> (psi)
$\omega$	rotation of $dV$

## DELTA ISOGRID STRUCTURE

The Delta launch vehicle project began in 1959 shortly after the formation of NASA. It started with existing stages that were comprised of the Thor first stage and Vanguard second and third stages. Since that time it has been project policy to upgrade the Delta booster for increased performance and reliability at a minimum cost growth as shown on figure 1. The current launch vehicle and improved configurations are shown on figure 2.

One of the many upgraded design features of these new Delta vehicles is the incorporation of a cylindrically shaped isogrid structure. This design forms the external skin structure of the booster. The new tank skin is initially machined from flat 1.27-cm (1/2-in.) thick 14ST6 free-machining aluminum alloy plate, brake-formed into curved shapes, and finally welded into 2.44-m (8-ft) diameter tank shells. Typical integrally machined structures, waffle and isogrid, are shown in figure 3. Isogrid now replaces the less efficient rectangular waffle tank and skin, stringer, and frame interstage and fairing structures. The improved Delta isogrid tank construction is about 50 percent more efficient (weightwise), than the waffle and equivalent in efficiency to the built-up assemblies with regards to compressive local and general buckling capabilities. It is also interesting to note that isogrid is orthogonally isotropic in its overall strain characteristics.

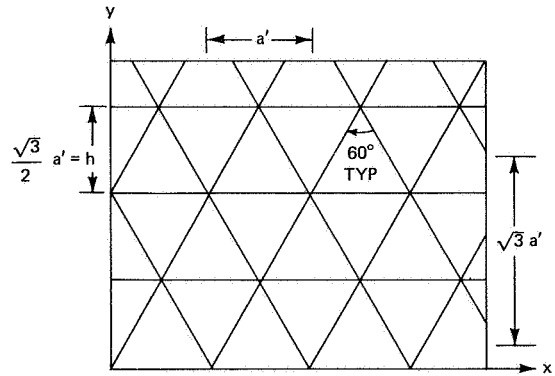
The first vehicles to employ the isogrid structure are now planned to carry the IMP H and TELESAT A spacecraft into orbit by the end of this year. Isogrid hardware is not only being fabricated for Delta vehicles but it is also being developed for the Shuttle (ref. 1) and Skylab programs under the cognizance of MSFC and is being proposed for more efficient Delta/Agena replacement second stages (fig. 4) in the Versatile Upper Stage (VUS) study (ref. 2) to GSFC requirements. Preliminary evaluations performed on Delta and the VUS indicate that isogrid structures are approximately 50 percent the cost of skin, stringer, and frame structures. This was the reason why the interstage and fairing were designed using isogrid for new model Deltas.

## ANALYSIS OF ISOGRID BY NASTRAN

The new structure, a relatively fine rib-node mesh, was modeled using NASTRAN program elements and procedures. Both static and buckling analysis were performed to give the Delta project a good understanding of the new structure being designed for Delta. Loadings applied to the isogrid model initially were only compression type but later were expanded to include pressure effects; i.e., hoop loadings. The compression loading included axial compression, equivalent axial compression due to bending, and offsetting axial tension forces  $pR/2$  due to internal pressure. The buckling analysis also included, for comparison only, the effects of an external pressure loading.

PROOF OF ISOTROPY OF ISOGRID

For an isogrid orientation having the  $a'$  and  $\sqrt{3}a'$  periodic grid distances shown to the right, it has been proven (ref. 3) that the material has isotropic elastic properties and that it obeys Hooke's law.



$$\sigma_x = \frac{\bar{E}}{1 - \nu^2} (\epsilon_{xx} + \nu \epsilon_{yy})$$

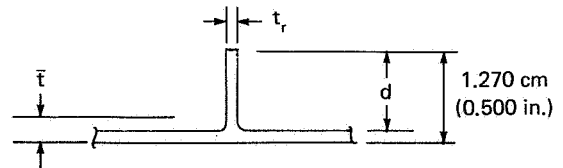
$$\sigma_y = \frac{\bar{E}}{1 - \nu^2} (\epsilon_{yy} + \nu \epsilon_{xx})$$

$$\tau_{xy} = \frac{\bar{E}}{1 + \nu} \epsilon_{xy}$$

where the isogrid elastic modulus  $\bar{E}$  is related to the actual material modulus  $E$  by  $\bar{E} = t_r E/h$ .

Subsequent to the previous analysis, the rib and plate elements were combined to produce an equivalent skin thickness  $\bar{t}$  such that the booster tank could be treated like an equivalent monocoque cylindrical structure. The equivalent monocoque skin thickness is

$$\bar{t} = t_s \left( 1 + \frac{t_r d}{t_s h} \right) = t_s + \frac{t_r d}{h}$$



The  $\bar{t}$  relation is important in solving for skin and rib compression allowables (ref. 4), which are

Skin buckling:

$$N_{sb} = 10.875 E \bar{t} \left( \frac{t_s}{h} \right)^2$$

$$f_{sb} = \frac{N_{sb}}{\bar{t}}$$

### Rib crippling:

$$N_{rc} = 0.422E\bar{t}\left(\frac{t_r}{d}\right)^2$$
$$f_{rc} = \frac{N_{rc}}{\bar{t}}$$

Isogrid, being isotropic, does possess an idiosyncrasy, i.e., its detail stresses must vary internally within the isogrid depending on the direction in which loadings are applied. The reason for this is that the isosceles triangular arrangement is oriented slightly differently in the x- and y-axis directions. To learn more about this novel structure, a small finite element model was fashioned using NASTRAN bar (CBAR) and triangular plate (CTRIA2) elements, figure 5. Specifically, this model was prepared to check the overall isotropic property of the integral rib and skin combination and to review the internal rib and skin stresses that result when the same magnitude of loading is placed in either the x or y directions.

The compression loading was selected from a typical Delta loading profile and is equated as follows:

$$N_x = \frac{P}{\pi D} + \frac{4M}{\pi D^2} = 308.2 \text{ kN/m (1760 lb/in.)}$$

$N_x$  was applied first in the negative x and then in the negative y directions. The results, including deflections and stress levels, are shown in figures 6 and 7. Note that the overall deflections, 1.346 mm (0.0530 in.), are the same for either x- or y-axis loadings, which indicates the overall isotropic characteristic of isogrid. Further, the rib and skin compressive stress levels in the center bay were lower for the x-axis loading direction (loads perpendicular to the main ribs) by 31 and 1 percent, respectively. Thus, to keep the compressive stresses at a minimum in the isogrid propellant tanks, the main ribs were located accordingly (on Delta stations, fig. 5).

The initial model, figure 5, was 46.94 cm (18.48 in.) square and required additional plate and bar elements. Two computer runs were made using heavy load support elements (50 times stiffer than isogrid CBAR members) and multiple point constraints at the load grid points and the same deflections and stress levels were obtained. The grid-point restraints are as noted on figure 6.

A third computer run was accomplished using a simpler model as shown in figure 8. Note that the model is 46.94 by 50.80 cm (18.48 by 20.00 in.) and contains fewer plate elements. The deflection and stresses are as shown in figures 9 and 10. The deflection and stresses are approximately the same as produced by the previous more complicated model. This simpler model was also utilized for the combined loading analysis, which is described in the next section.

## COMBINED LOADING OF ISOGRID

The previous NASTRAN models were loaded in compression only. Next, the preceding model, having a single fixed point (grid point 28), was loaded with axial compression (308.2 kN/m (1760 lb/in.)) and hoop tension (414 kN/m<sup>2</sup> (60 psi)) forces. For the levels of loading applied, the results are as shown in figures 11 and 12. The rib compressive stress level was 51 percent lower and the skin buckling level was 3 percent higher for the x-axis loading conditions where the compression loadings were perpendicular to the main ribs (fig. 11). A close look at the actual rib and skin stresses and a direct comparison with their respective allowable stresses is given in table 1. Note that the skin actual stress was closer to its allowable stress. For the combined loads case analyzed, the skin stress will be a minimum if the compression load is in line with the isogrid main rib. Because past tests (ref. 5) indicate that local skin buckling will reduce general instability allowables (by approximately 20 percent), it is important to keep the skin actual stresses as low as possible.

TABLE 1.--Rib and Skin Compression Stresses

Element	Actual stress, kN/m <sup>2</sup> (psi)	Allowable stress, kN/m <sup>2</sup> (psi)	$\left(\frac{\text{Allowable stress}}{\text{Actual stress}} - 1\right) 100,$ percent
Rib	-252 067 (-36 558)	-424 042 (14ST651 yield corrected for plasticity; -61,500)	+68
Skin	-173 637 (-25 183)	-202 024 (-29 300)	+16

## LIAISON COMPUTER ANALYSIS

During the early stages of fabrication, there have been occasions when isogrid skins have been machined improperly. In the cases where skin pockets and rib thicknesses were undersized at random locations, the small NASTRAN model previously described was used effectively. Having the actual stress levels throughout the model, it was quite easy to determine rib and skin margin of safety and whether reinforcements were required.

ISOGRID TANK STATIC AND BUCKLING ANALYSIS  
(MOVE AND NASTRAN PROGRAMS)

This analysis was performed to determine the general instability theoretical allowables for axial compression and various tank hydrostatic loadings; i.e., negative or external, zero, or positive or internal pressure loadings.

The fact that tank pressure loading can be handled quite easily by the NASTRAN program made this a more interesting and comprehensive study. The results of this analysis compared with test data and other methods of analysis (ref. 6) will be summarized later. Before discussing the model and the results, a brief description of the theory will be presented.

BUCKLING THEORY

NASTRAN buckling analysis (ref. 7) is based on the elastic and differential stiffnesses of the structure analyzed. The elastic properties of a structure are generally dependent on shear  $AG/K$ , torsion  $JG$ , bending  $EI$ , and axial  $AE$  stiffness characteristics. The differential stiffness is based on the static loading, displacement, and geometry of the structure. An example of a bar element differential stiffness matrix is shown in figure 13 (ref. 7). The approach presented in reference 7 is essentially based on using Lagrange's equations of motion on a structural system with a finite number of degrees of freedom.

The steps (ref. 7) for including differential stiffness in a structural problem are as follows:

- (1) Solve the linear static response problem for the structure in the absence of differential stiffness and compute the internal forces in each element.
- (2) Using the results of (1), calculate the differential stiffness matrix for the individual elements and apply the standard reduction procedure (constraints and partitioning) to form the differential stiffness matrix  $[K_{aa}^d]$  in final form.
- (3) For the buckling problem, find the characteristic eigenvalue and eigenvectors for

$$[K_{aa} + \lambda K_{aa}^d] \{u\} = 0$$

For the isogrid cylinder buckling problem, the inverse power method was used to determine the eigenvalues. Because the above-defined set of buckling equations are homogeneous, the assignment of one arbitrary eigenvector (within NASTRAN) must be made to start the analysis. The solution of the first trial eigenvalue permits the determination for convergence; the redetermination of the eigenvalue, if necessary; and the subsequent final solution of all eigenvector ratios  $\{u\}$  or of the mode shape.



It is the eigenvalue that is the factor by which the applied compression static loading is multiplied to produce the theoretical threshold of buckling. Once obtained, the theoretical buckling load is multiplied by a 65-percent reduction factor. That factor has evolved from testing full-scale isogrid cylinders and it accounts for manufacturing tolerances and distortions that are present in hardware.

#### BUCKLING MODEL DESCRIPTION

During June 1971, three isogrid tank segments (244-cm diameter by 244-cm length (8-ft diameter by 8-ft length)) were fabricated from free-machining 2014T6 aluminum; subsequently, compression tested with zero internal pressure. The mathematical model was determined, based on those compression test tank sizes, in order to correlate computer results with test values.

The NASTRAN model, being an exact replica of the tested tank segments, was a rather fine and detailed model. This model size is believed to be the largest structural model analyzed at NASA Goddard Space Flight Center. The model was composed of NASTRAN triangular plate (CTRIA2) and bar (CBAR) elements. A complementary computer program, MOVE (ref. 8), was utilized to simplify the task. A model such as ours, having 1850 grid points and 7986 elements, would have been extremely difficult, if not impossible within the time available, to construct had it not been for the help of the MOVE program.

The MOVE program was designed to generate repeat bulk data for structures having a number of identical segments. All one need do is to generate one basic NASTRAN bulk data segment and MOVE does the rest. The strip model selected for our problem was a longitudinal segment shown in figure 14. By moving that segment 66 times ( $5.45^\circ$  per move circumferentially), the complete cylinder was generated as shown in figure 15. It should be noted here that all of the undeformed and deformed figures in this report were made by the Stromberg-Carlson 4060 plotter, which is one of several systems that may be specified in NASTRAN programming.

When the MOVE program was first programmed, it was designed for a relatively small structural problem. Thus, the initial trial of that program on a large structural model was not successful. The reason was that the MOVE program could not handle CBAR continuation cards and a very large number of repeat cycles. Further, the MOVE program was written to place its bulk data output on punched cards. This feature could have been quite cumbersome to handle for our large buckling problem (approximately 8 data card file boxes, or 8000 cards). Including the output data on tape was a far superior way of handling an immense quantity of data. That program, written in PL-1 language, was subsequently revised to rectify the above problem areas and to store its output data on magnetic tape.

Having accomplished the MOVE programming successfully, the next step was to input the data using NASTRAN programming methods. Here too, initial attempts were not good because of an assortment of program problems involving the

application of the MOVE data tape and the determination of a practical size storage requirement for our isogrid structural model. The solutions were readily available by properly arranging the executive control section of NASTRAN and adjusting the storage requirement from 500 000 to 1 000 000 places. Incidentally, the isogrid tank buckling computer analysis required all but 5000 places for some of the NASTRAN routines--that was measuring storage quite close. Yet still another problem occurred: The computer program timed out at 120 min of requested central processing unit (CPU) time. Rather than increase the run time, the model was reduced, but reduced in such a way that the original size tank configuration could be maintained. This was achieved by reducing the NASTRAN model to one-quarter the original size, limiting the buckling problem by analyzing only the first four symmetric-symmetric modes as shown in figure 16, and establishing the constraints or degrees of freedom accordingly.

To accomplish the reduction in model size to one-quarter the original, the grid points were modified to include 1 through 13 (fig. 14) only and the MOVE rotations ( $5.45^\circ$ /rotation) were reduced from 66 to 33. The MOVE program was rerun and the reduced data (on tape) were submitted via NASTRAN for a plot of the one-quarter-scale model shown in figure 17.




The buckling analysis was again attempted and constraint problems were encountered. A more careful look at the symmetric-symmetric modes and the loaded end conditions led to grid-point degrees of freedom revisions that subsequently produced good buckling results as shown in table 2. Plots of the statically deformed and buckled structure are presented in figures 18 to 24.

But how dependable was the general instability buckling analysis using NASTRAN? To answer this question, the NASTRAN output was compared directly to another analysis (ref. 6) and to isogrid tank compression test data (refs. 4 and 9) as shown in figure 25. For that figure the theoretical buckling values were multiplied by a 65-percent test correlation factor (ref. 4) and compared to 99 percent probability buckling test values (2.340 lower than the average of nine test data points). The lower than theoretically predicted buckling allowables thus achieved account for imperfections that are inherent in large structures. Such imperfections are generally attributable to built-in residual forming stresses, slight amounts of tank out-of-roundness, and local rib and skin waviness.

Figure 25 graphically documents instability buckling levels for the Delta isogrid and waffle designs as compared to monocoque designs. It also shows the allowable skin buckling running load for the isogrid design. The graph has been produced by placing the weight equivalent thickness ( $t_{wt. eq.}$ ) along the abscissa and the allowable compressive load ( $N_{GI}$  or  $N_{sb}$ ) along the ordinate.

By scanning figure 25, it becomes apparent that the general instability allowables obtained through the use of NASTRAN correlate very well with the test data point and the cylindrical shell analysis by W. Flugge (ref. 6) and McDonnell Douglas H312 analysis. Because the symmetric-symmetric buckling results appeared to be quite good, further analyses in the asymmetric buckling modes were not performed.

TABLE 2.--Isogrid Tank Structure NASTRAN Buckling Analysis Data

Item no.	Loading condition	Run time, min		Rigid format	Date of run	Output		Maximum compression N, kN/m (lb/in.)	Theoretical buckling N, kN/m (lb/in.)	NGI = 0.65 AN, kN/m (lb/in.)
		CPU	I/O			Modes	Eigen-value, $\lambda$			
1	414-kN/m <sup>2</sup> (60-psi) uniform external pressure plus unsymmetrical compression loads 	84	79	12.1.1	1/8/72	12	1.042	302.8 (1730)	315.5 (1803)	204.8 (1170)
2	414-kN/m <sup>2</sup> (60-psi) uniform internal pressure plus unsymmetrical compression loads 	65	72	12.1.2	2/5/72	3	1.433	302.8 (1730)	433.8 (2479)	281.8 (1610)
3	Unsymmetrical compression loads 	41	46	12.1.2	3/11/72	1	1.338	302.8 (1730)	405.1 (2315)	263.4 (1505)

Note also that the instability plots are based on compression loadings and no internal pressure. To verify the pressure effect, analysis was performed using NASTRAN for the conditions of compression loading and  $414\text{-kN/m}^2$  (60-psi) internal and external pressure. These data points are also shown in figure 25. It is interesting to observe that internal pressure (through pressure stiffening of skin and rib) improves the zero-pressure buckling allowable by 7 percent, and the external pressure degrades the zero-pressure buckling level by -22 percent. The 7-percent improvement correlates fairly well with a 4-percent gain seen during testing of scaled-down lexan isogrid models (ref. 5).

Observe also that isogrid is local skin buckling critical from a thickness of 2.39 mm (0.093 in.) and lower. During the previously mentioned scaled-down lexan isogrid test program, local skin buckling levels with and without internal pressure were evaluated. The results are what would be expected--the general instability buckling load level was improved by 20 percent by adding an internal pressure loading. The reason for that improvement was that internal pressure stiffened the ribs and skin pocket areas such that 100 percent of the theoretical general instability level could be achieved. It is for this reason that a combined loads (compression, shear, and internal pressure) research and development task has been proposed. The combined loads would be applied to several full-scale aluminum isogrid tank segments (2.44-m diameter by 2.44-m length (8-ft diameter by 8-ft length)).

#### CONCLUSIONS

The NASTRAN program techniques have been advantageously employed on the Delta launch vehicle isogrid structure in the following areas:

- (1) The combined loads isogrid model served as an excellent analytical tool in accomplishing liaison stress analysis. That isogrid is orthogonally isotropic was proved by NASTRAN.
- (2) NASTRAN buckling analysis produces good general instability buckling allowable load levels. It also has the capability of combining axial compression, bending, shear, and pressure loadings. Shear effects were omitted in this analysis in order to correlate test and other analyses.
- (3) Buckling analysis of the isogrid cylinder determined that internal pressure loading, when combined with axial compression loading, provides a 7-percent improvement in the general instability allowable. Because both local skin pocket and instability buckling allowables are improved by internal pressure stiffening effects, a combined loads development task has been proposed.

## ACKNOWLEDGMENTS

The author wishes to acknowledge the assistance of Margorie Johns (NASA GSFC) and William Gorman and Karl Swenson (Computer Sciences Corp. at GSFC) for their work on the MOVE and NASTRAN program support phases. Recognition is also given to Robert Meyer (McDonnell Douglas) for the many years of research in isogrid development and for his enthusiastic assistance. In addition, special thanks go to Thomas Butler (NASA GSFC) for his help in the theory behind NASTRAN and in his encouragement during the course of this analytical study.

## REFERENCES

1. Meyer, R. R.: Booster Airframe. Pt. III of Space Shuttle Data, Rept. MDC EO375, McDonnell Douglas, June 30, 1971.
2. Nelson, L. M.; et al.: Phase A Advanced Versatile Upper Stage (VUS) Study. Vol. I, Tech. Book I, Astronautics Rept. GD/CA BNZ72-006, General Dynamics/Convair, May 1972.
3. Meyer, R. R.; and Bellifante, R. J.: Isotropic Analysis. Pt. I of Fabrication and Experimental Evaluation of Common Domes Having Waffle-Like Stiffening, Rept. SM-47742, Douglas Aircraft Corp., Nov. 1964, p. 78.
4. Chen, R.: Isogrid Strength Allowables--Delta Booster Tanks and Interstage. Rept. MDC G2833, McDonnell Douglas, Apr. 1972.
5. Jenkins, W. C.: Determination of Critical Buckling Loads for Isogrid Stiffened Cylinders. Rept. MDC G2792, McDonnell Douglas, Feb. 1972.
6. Flugge, W.: Stresses in Shells. Springer Verlag (Berlin), 1962.
7. MacNeal, Richard H.: NASTRAN Theoretical Manual. NASA SP-221, Sept. 1970.
8. Cook, W. L.: Automated Input Data Preparation for NASTRAN. NASA TM X-63607, Apr. 1969.
9. Sternitzke, J. F.: (DELTA) Isogrid Cylinder Buckling Capabilities.. Vol. I, Rept. MDC G2472, McDonnell Douglas, Aug. 1971.

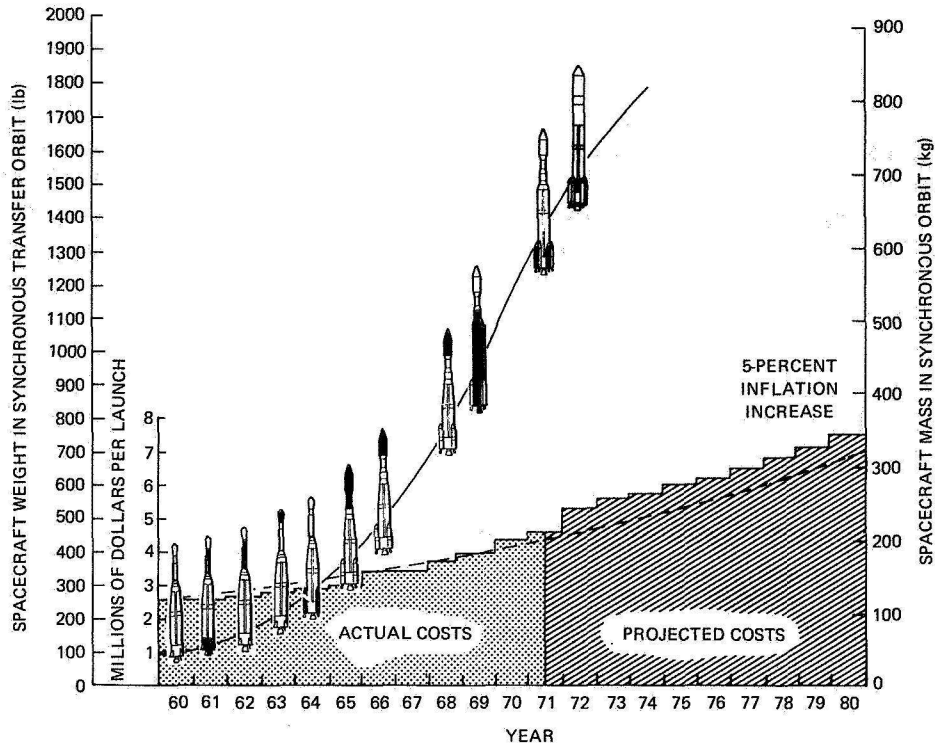


Figure 1.--Delta performance and cost history.

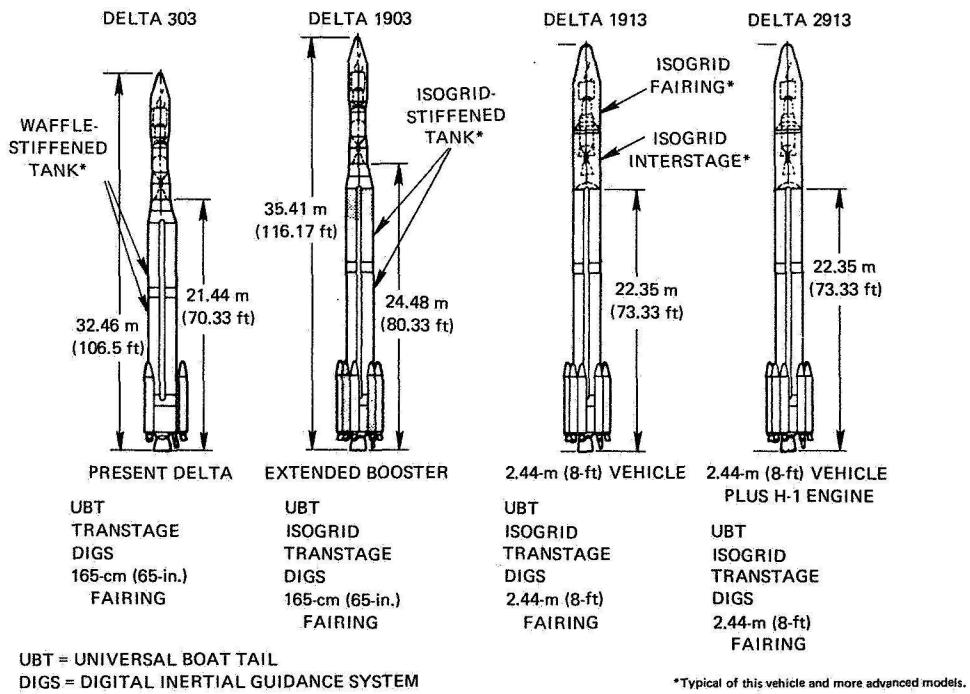


Figure 2.--Configuration development plan.

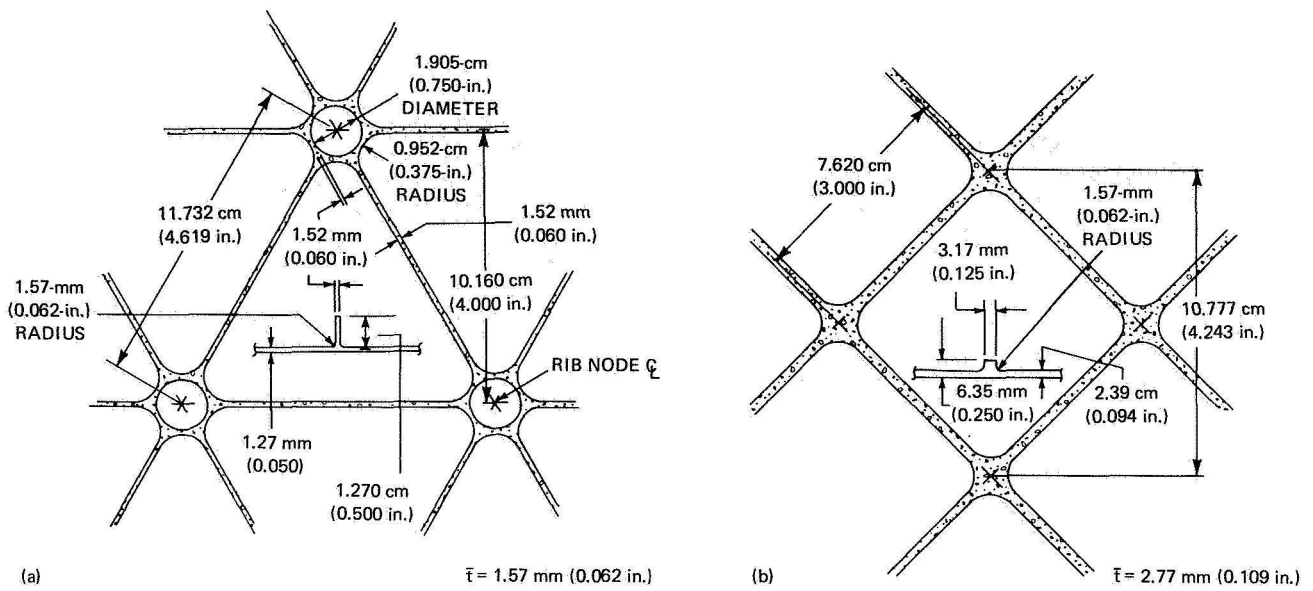


Figure 3.--Thor tank grid pattern. (a) Isogrid. (b) Waffle.

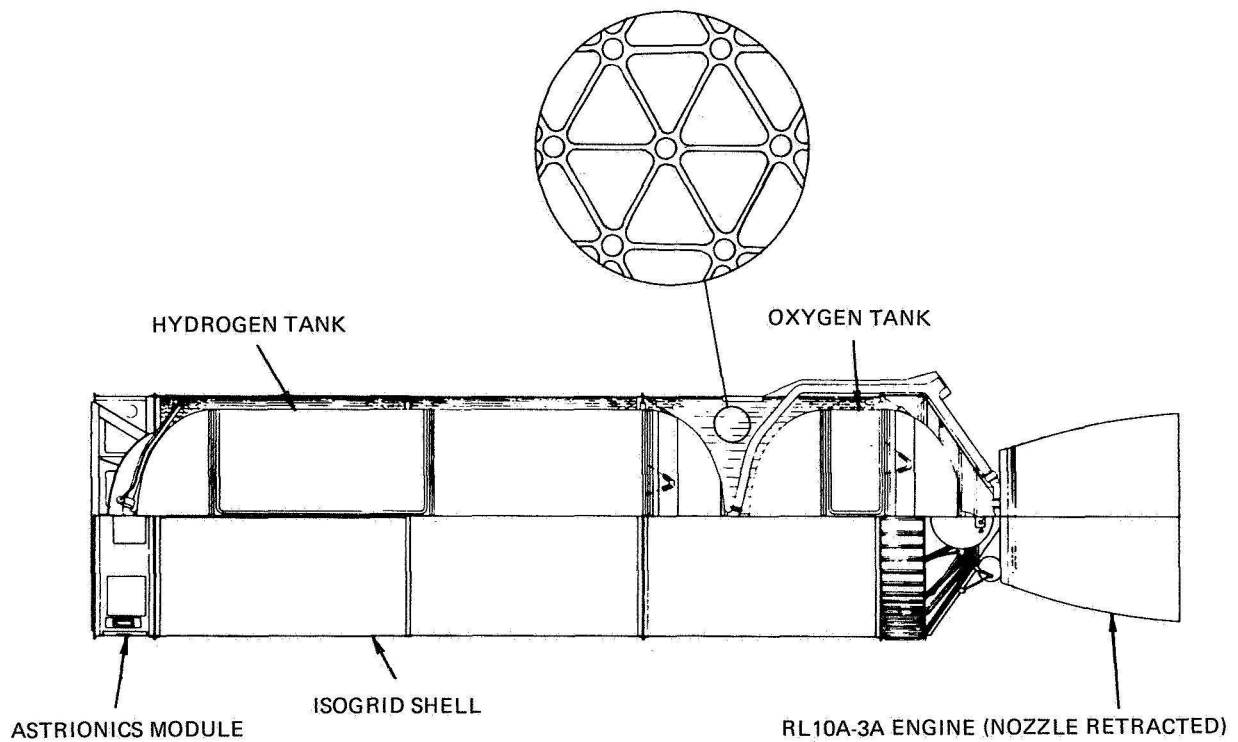


Figure 4.--Delta/Agena replacement stage.

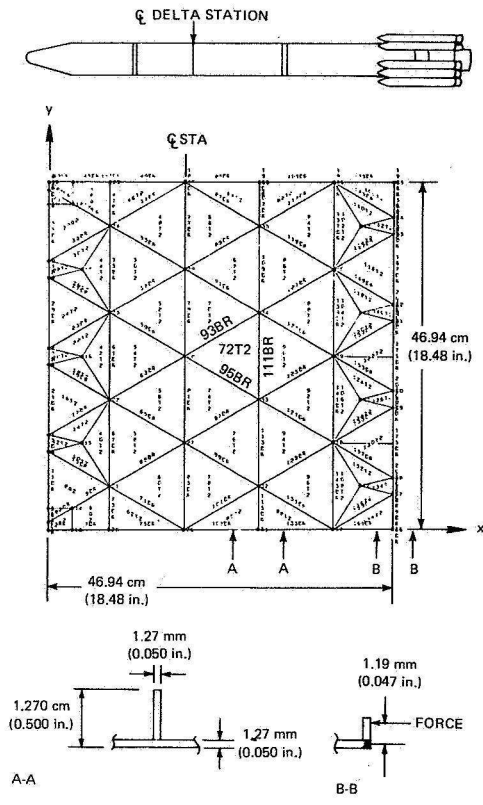


Figure 5.--Delta isogrid NASTRAN model .

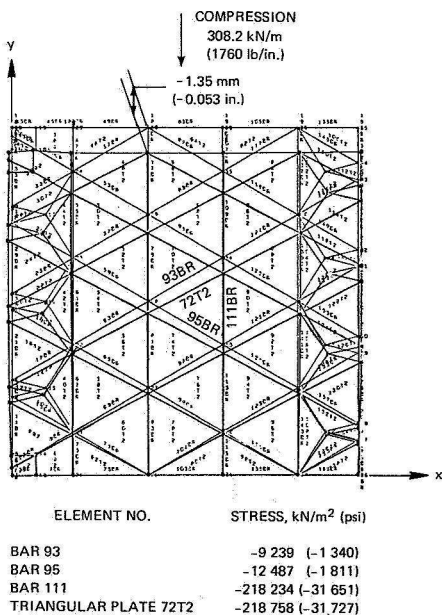


Figure 7.--Deflection and stresses, compression load in -y direction.

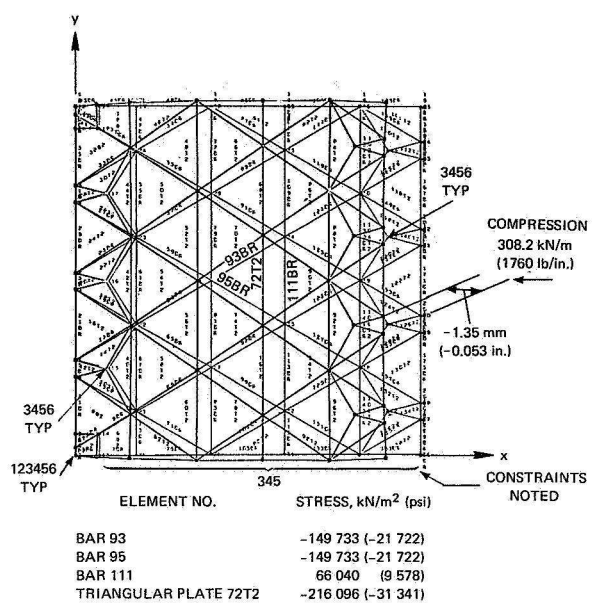


Figure 6.--Deflection and stresses, compression load in -x direction.

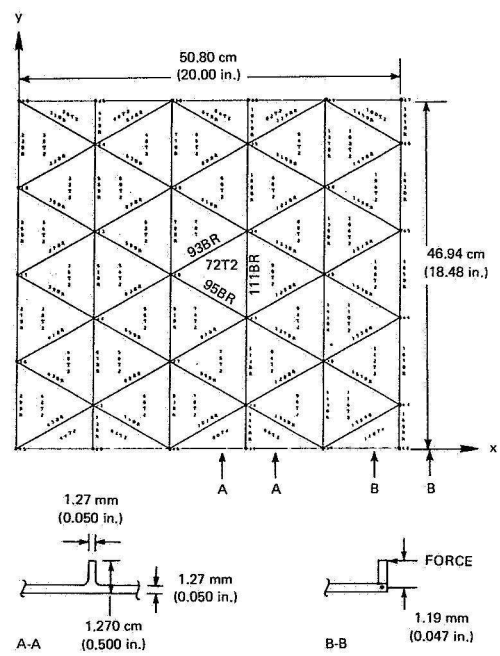
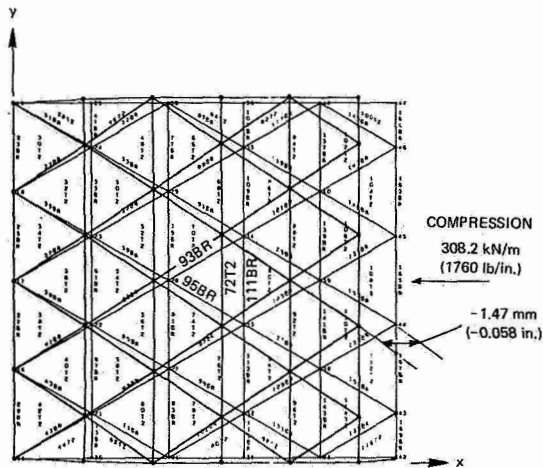


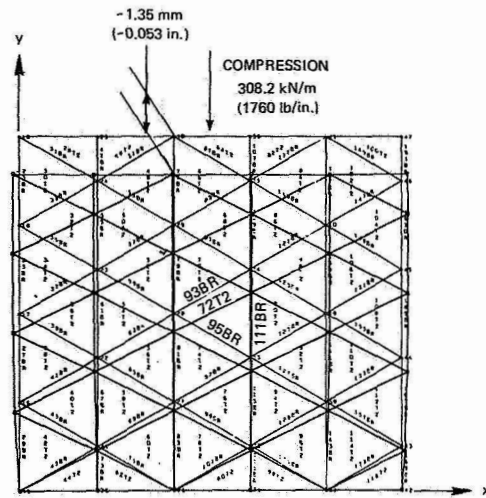
Figure 8.--Delta isogrid NASTRAN model (simplified).





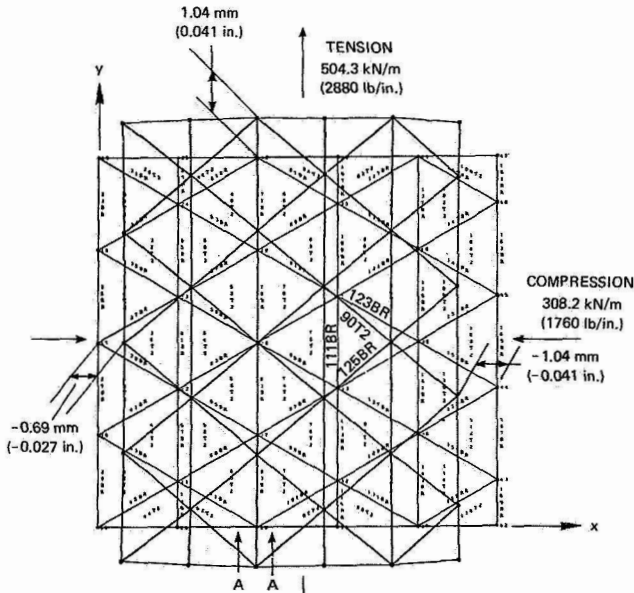
ELEMENT NO.	STRESS, kN/m <sup>2</sup> (psi)
BAR 93	-153 993 (-22 334)
BAR 95	-153 993 (-22 334)
BAR 111	64 737 (9 389)
TRIANGULAR PLATE 72T2	-222 198 (-32 226)

Figure 9.--Deflection and stresses, compression load in -x direction.



ELEMENT NO.	STRESS, kN/m <sup>2</sup> (psi)
BAR 93	-6 592 (-956)
BAR 95	-14 459 (-2 097)
BAR 111	-217 944 (-31 609)
TRIANGULAR PLATE 72T2	-219 309 (-31 807)

Figure 10.--Deflection and stresses, compression load in -y direction.



ELEMENT NO.	STRESS, kN/m <sup>2</sup> (psi)
BAR 123	-122 055 (-17 702)
BAR 125	-122 055 (-17 702)
BAR 111	327 954 (47 564)
TRIANGULAR PLATE 90T2	-173 637 (-25 183)

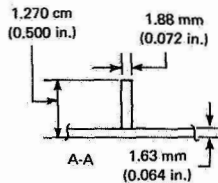
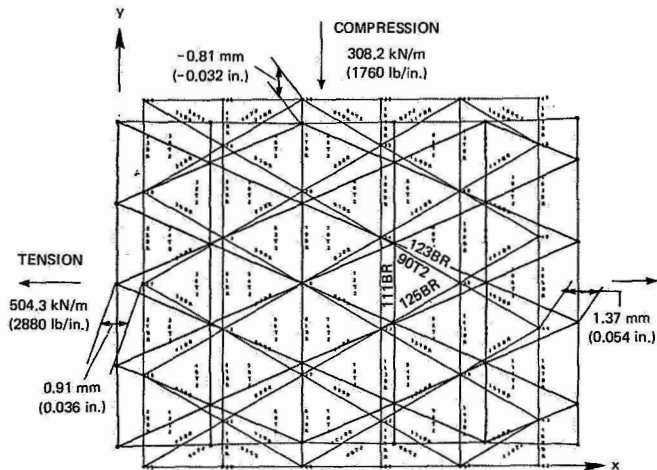
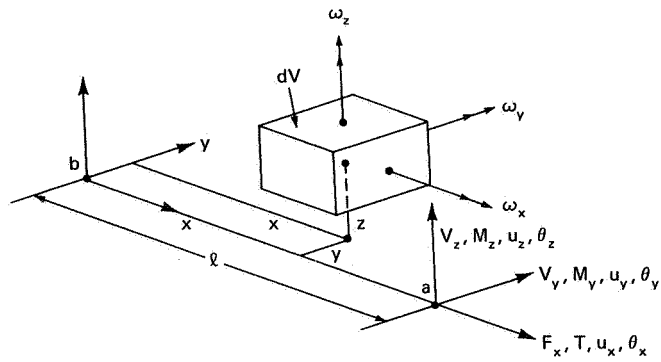


Figure 11.--Deflection and stresses, compression and tension loadings (tension parallel to main ribs).



ELEMENT NO.	STRESS, kN/m <sup>2</sup> (psi)
BAR 123	196 473 (28 495)
BAR 125	196 473 (28 495)
BAR 111	-252 067 (-36 558)
TRIANGULAR PLATE 90T2	-168 059 (-24 374)

Figure 12.--Deflection and stresses, compression and tension loadings (compression parallel to main ribs).



$$[K_{aa} + \lambda K_{aa}^d] \{u\} = 0$$

$$\begin{Bmatrix} f_{ya} \\ f_{za} \\ m_{xa} \\ m_{ya} \\ m_{za} \\ f_{yb} \\ f_{zb} \\ m_{xb} \\ m_{yb} \\ m_{zb} \end{Bmatrix} = \begin{bmatrix} \frac{6F_x}{5l} & 0 & \frac{M_{yb}}{l} & 0 & -\frac{F_x}{10} & -\frac{6F_x}{5l} & 0 & \frac{M_{ya}}{l} & 0 & -\frac{F_x}{10} \\ 0 & \frac{6F_x}{5l} & \frac{M_{zb}}{l} & \frac{F_x}{10} & 0 & 0 & -\frac{6F_x}{5l} & \frac{M_{za}}{l} & \frac{F_x}{10} & 0 \\ \frac{M_{yb}}{l} & \frac{M_{zb}}{l} & \frac{IF_x}{l^2A} & -\frac{lV_y}{6} & -\frac{lV_z}{6} & -\frac{M_{yb}}{l} & -\frac{M_{zb}}{l} & -\frac{IF_x}{l^2A} & \frac{lV_y}{6} & \frac{lV_z}{6} \\ 0 & \frac{F_x}{10} & -\frac{lV_y}{6} & \frac{2l}{15}F_x & 0 & 0 & -\frac{F_x}{10} & \frac{lV_y}{6} & -\frac{lF_x}{30} & 0 \\ -\frac{F_x}{10} & 0 & -\frac{lV_z}{6} & 0 & \frac{2l}{15}F_x & \frac{F_x}{10} & 0 & \frac{lV_z}{6} & 0 & -\frac{lF_x}{30} \\ -\frac{6F_x}{5l} & 0 & -\frac{M_{yb}}{l} & 0 & \frac{F_x}{10} & \frac{6F_x}{5l} & 0 & -\frac{M_{ya}}{l} & 0 & \frac{F_x}{10} \\ 0 & -\frac{6F_x}{5l} & -\frac{M_{zb}}{l} & -\frac{F_x}{10} & 0 & 0 & \frac{6F_x}{5l} & -\frac{M_{za}}{l} & -\frac{F_x}{10} & 0 \\ \frac{M_{ya}}{l} & \frac{M_{za}}{l} & -\frac{IF_x}{l^2A} & \frac{lV_y}{6} & \frac{lV_z}{6} & -\frac{M_{ya}}{l} & -\frac{M_{za}}{l} & \frac{IF_x}{l^2A} & -\frac{lV_y}{6} & -\frac{lV_z}{6} \\ 0 & \frac{F_x}{10} & \frac{lV_y}{6} & -\frac{lF_x}{30} & 0 & 0 & -\frac{F_x}{10} & -\frac{lV_y}{6} & \frac{2lF_x}{15} & 0 \\ -\frac{F_x}{10} & 0 & \frac{lV_z}{6} & 0 & -\frac{lF_x}{30} & \frac{F_x}{10} & 0 & -\frac{lV_z}{6} & 0 & \frac{2lF_x}{15} \end{bmatrix} \begin{Bmatrix} u_{ya} \\ u_{za} \\ \theta_{xa} \\ \theta_{ya} \\ \theta_{za} \\ u_{yb} \\ u_{zb} \\ \theta_{xb} \\ \theta_{yb} \\ \theta_{zb} \end{Bmatrix}$$

Figure 13.--Prismatic beam and differential stiffness.

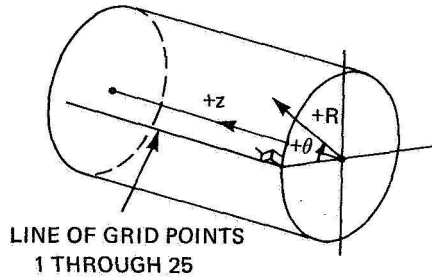
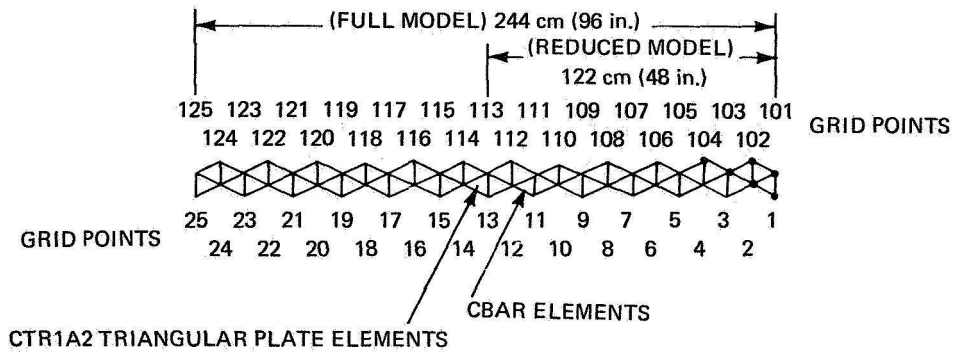


Figure 14.--NASTRAN segment for MOVE program.

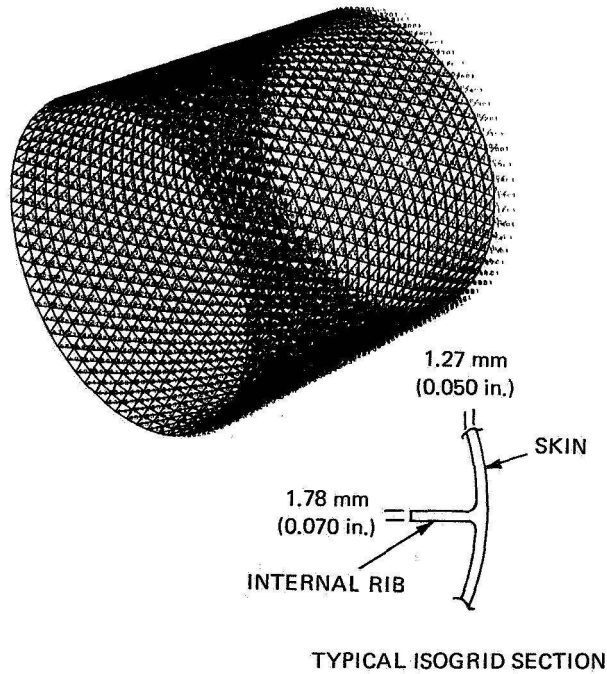


Figure 15.--Isogrid tank structural model (1850 grid points; 7986 elements).

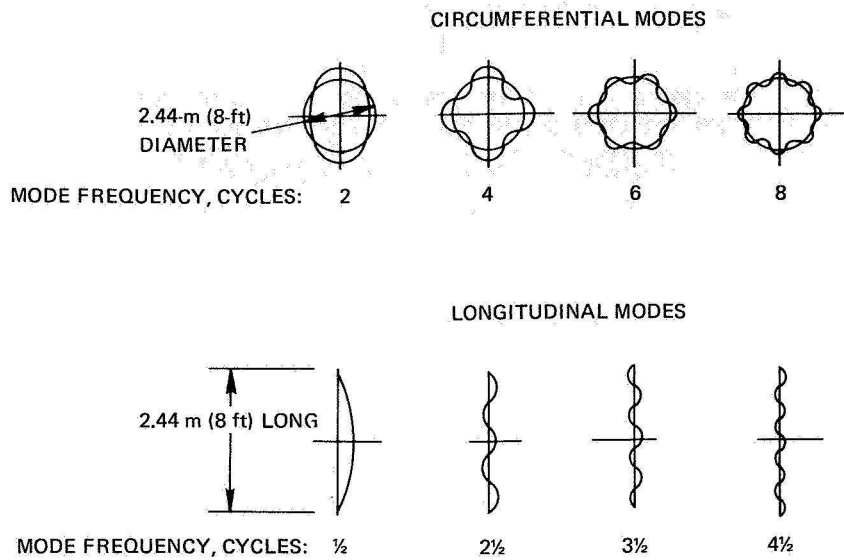


Figure 16.--Symmetric-symmetric modes for isogrid tank 2.44 m (8 ft) in diameter and 2.44 m (8 ft) in length.

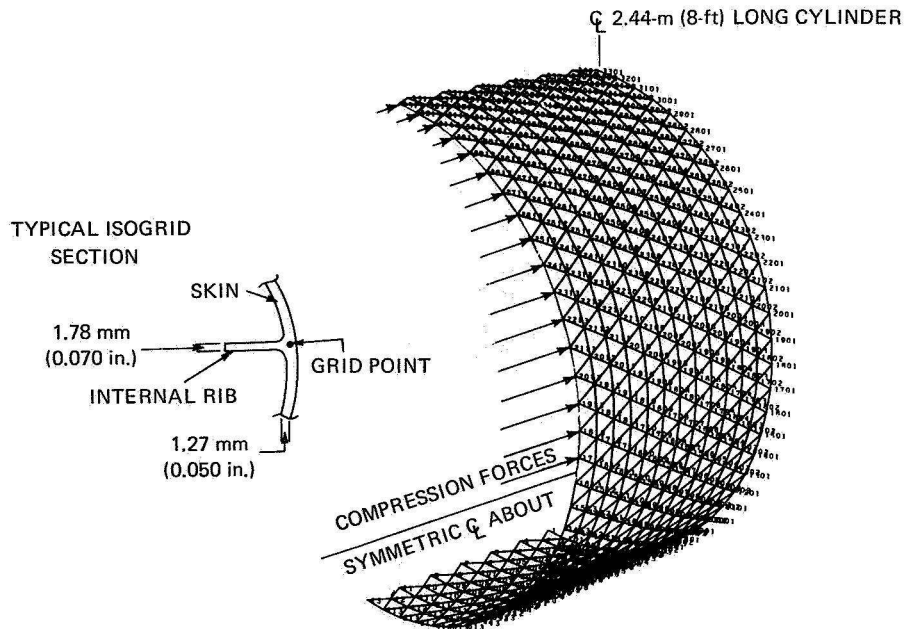


Figure 17.--One quarter tank model undeformed (1.2-m (4-ft) length, 1.2-m (4-ft) radius). Axial compression forces include bending moment equivalent force, axial force, and offsetting pressure equivalent force.

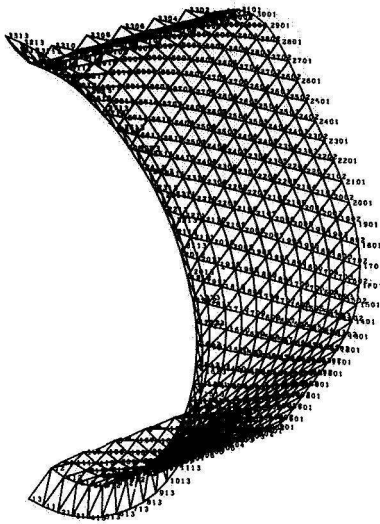


Figure 18.--Static deflections, compression load plus  $414\text{-kN/m}^2$  ( $60\text{-psi}$ ) external pressure.

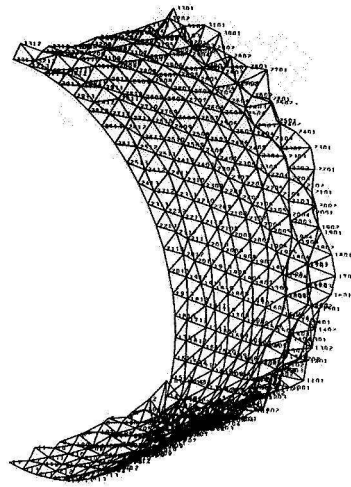


Figure 19.--First buckling mode, compression load plus  $414\text{-kN/m}^2$  ( $60\text{-psi}$ ) external pressure.

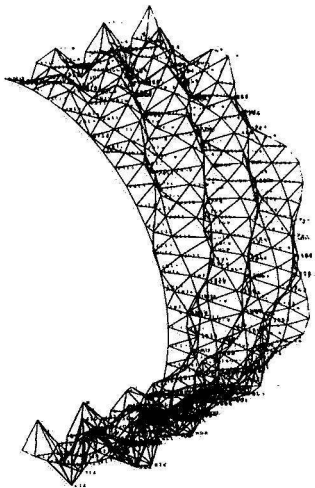


Figure 20.--Second buckling mode, compression load plus  $414\text{-kN/m}^2$  ( $60\text{-psi}$ ) external pressure.

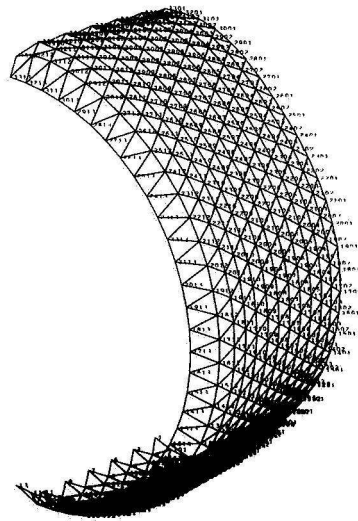


Figure 21.--Static deflections, compression load plus  $414\text{-kN/m}^2$  ( $60\text{-psi}$ ) internal pressure.

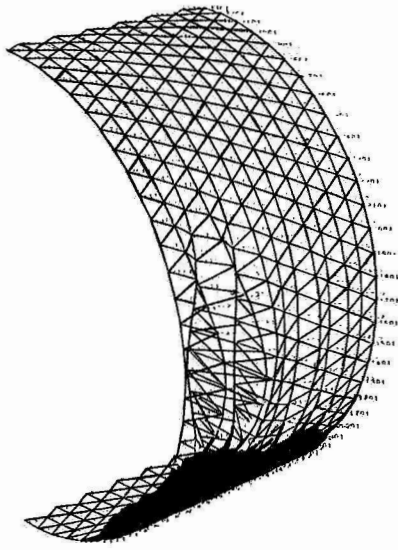


Figure 22.--First buckling mode, compression load plus 414-kN/m<sup>2</sup> (60-psi) internal pressure.

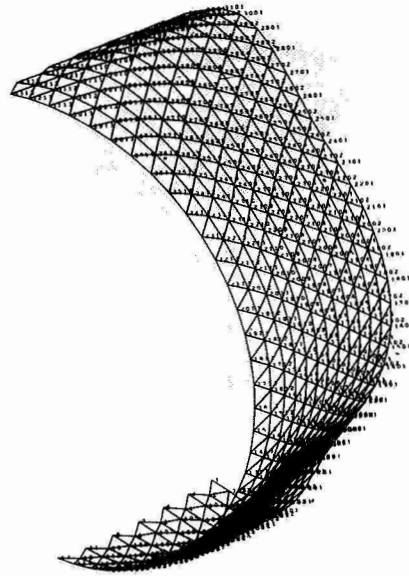


Figure 23.--Static deformation, compression load plus zero internal pressure.

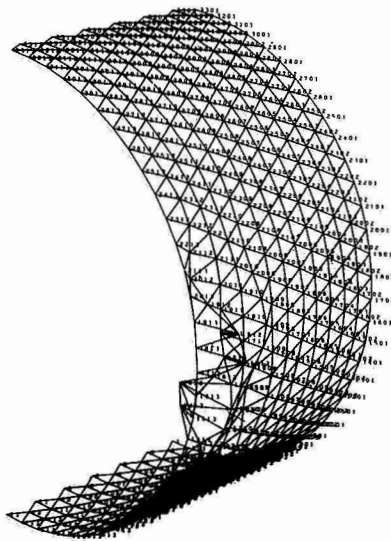


Figure 24.--First buckling mode, compression load plus zero internal pressure.

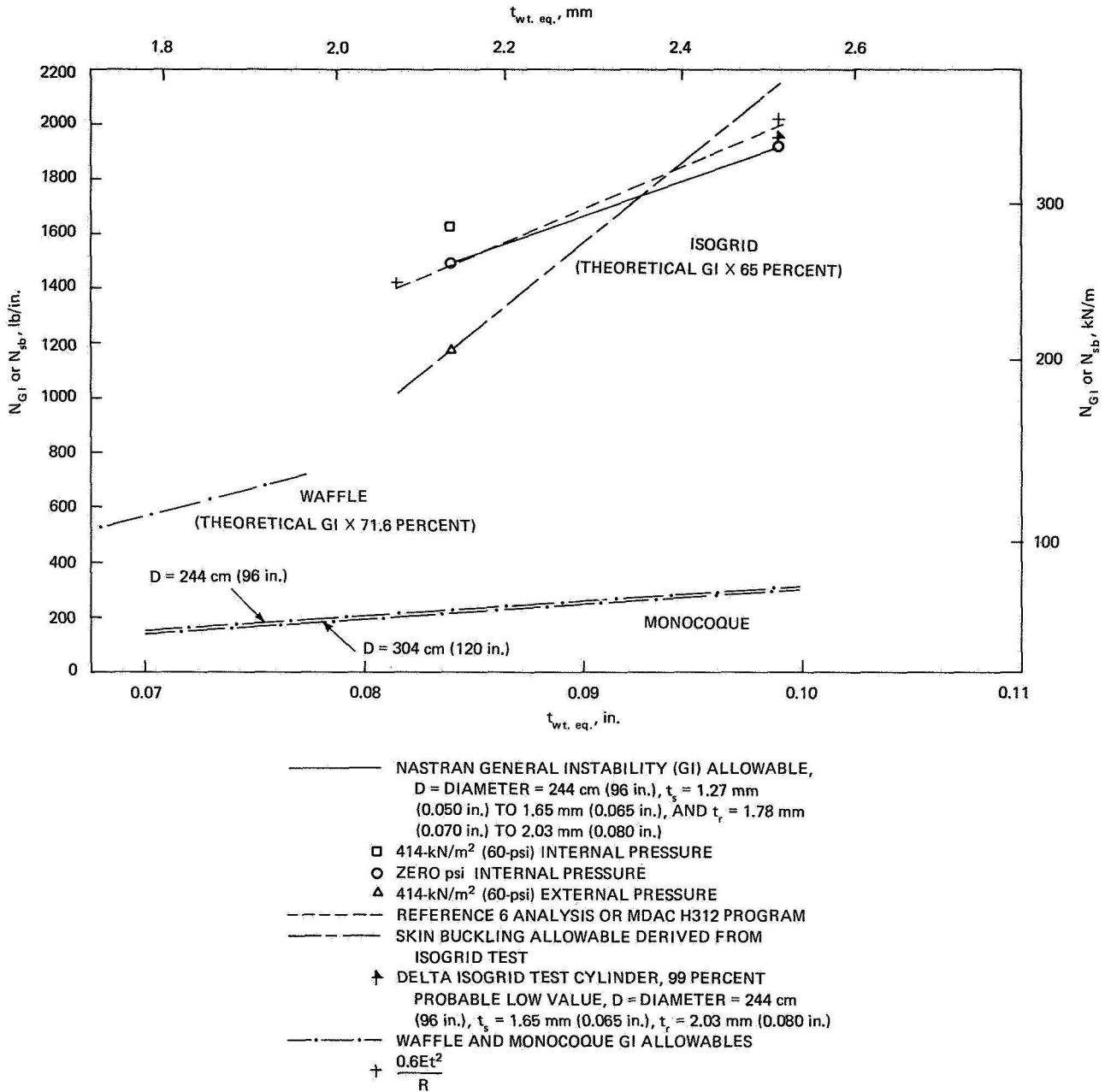


Figure 25.--Buckling allowables, 14ST6 aluminum cylinders.